

ABSTRACT

MACLEOD, MARC. Dynamic Modeling, Analysis, and Testing of a Variable Buoyancy System for Unmanned Multi-Domain Vehicles. (Under the direction of Dr. Matthew Bryant).

This paper presents the system design and dynamic model of an active variable buoyancy system (VBS) actuator with applications to unmanned multi-domain vehicles. Unmanned multi-domain vehicles have a unique concept of operations that require nontraditional VBS designs. We present a VBS actuator design that focuses on vehicle design objectives of high endurance, stealth, and loitering while underwater. The design consists of an elastic bladder housed within a rigid ballast tank, hydraulic pump, and proportionally controlled vent valve. Ambient surrounding water is the system working fluid and the elastic bladder serves to separate the gas–water interface, eliminating the risk of the compressed gas escaping when venting the water during extreme pitch maneuvers. A nonlinear analytic model of the VBS is derived and used to examine the parameter design space and the effects on water flow rate, actuation force, and energy efficiency. The VBS actuator design is shown to require a smaller, denser energy storage device than a comparable buoyancy system that uses consumable compressed air. A vehicle model is studied that features forward and aft VBS actuators, which enables vehicle pitch control by shifting the center of gravity along the vehicle’s longitudinal axis. The coupling between the VBS actuator dynamics and vehicle dynamics are presented and discussed. A proof-of-concept demonstration is presented and compared to the analytical system model.

© Copyright 2015 Marc MacLeod

All Rights Reserved

Dynamic Modeling, Analysis, and Testing of a Variable Buoyancy
System for Unmanned Multi-Domain Vehicles

by
Marc MacLeod

A thesis submitted to the Graduate Faculty of
North Carolina State University
in partial fulfillment of the
requirements for the degree of
Master of Science

Mechanical Engineering

Raleigh, North Carolina

2015

APPROVED BY:

Dr. Matthew Bryant
Committee Chair

Dr. Ashok Gopalarathnam

Dr. Kara Peters

BIOGRAPHY

Marc MacLeod is the man.

ACKNOWLEDGMENTS

I gratefully acknowledge funding support from DARPA and Teledyne Scientific Company, without which the present research could not have been completed. I thank my committee members for their support and the rest of my student research team for their help in making this project a success. I also thank iSSRL for providing the lab space and equipment necessary for completion of the project. Finally I thank my advisor Dr. Matthew Bryant for his endless support and guidance, which was critical to this research.

TABLE OF CONTENTS

LIST OF TABLES	v
LIST OF FIGURES	vi
1. INTRODUCTION	1
<i>1.1. Brief Survey of Multi-Domain Vehicle Designs</i>	1
<i>1.2. Buoyancy Control for UUVs</i>	5
<i>1.3. Proposed VBS Actuator</i>	8
2. VARIABLE BUOYANCY SYSTEM MODEL	9
<i>2.1. System Configuration</i>	9
<i>2.2. Dynamic System Model</i>	11
<i>2.3. Variable Buoyancy System Actuator Analysis</i>	14
3. MODEL ANALYSIS RESULTS AND DISCUSSION	16
4. COMPARISON TO CONSUMABLE COMPRESSED AIR BUOYANCY SYSTEM	22
5. HOW TO SIZE THE BALLAST TANK	26
6. DYNAMIC VEHICLE SYSTEM MODEL	32
<i>6.1. System Configuration</i>	32
<i>6.2. Nonlinear System Model</i>	34
7. VEHICLE SYSTEM DYNAMIC RESULTS	37
8. PROOF-OF-CONCEPT DEMONSTRATION	41
9. CONCLUSIONS	48
REFERENCES	50

LIST OF TABLES

Table 1. Baseline parameters of the VBS Actuator	16
Table 2. Typical commercially available compressed air tank specifications	25
Table 3. VBS Test Platform II component approximations.....	33

LIST OF FIGURES

Figure 1. VBS ballast tank operating concept.....	10
Figure 2. Maximum bidirectional actuation force as a function of vehicle depth limit for tank pressure limits from 5 to 25 bar in 4 bar increments.	17
Figure 3. Ballast tank fill fraction limit as a function of vehicle depth for 0.7 ml/rev pump displacement and applied voltages from 12 to 28 volts in 4 volt increments. Results shown for tank precharges [depth limits] of 2.7 bar [15 m], 4.4 bar [30 m] and 7.6 bar [60 m].	18
Figure 4. Ballast tank fill fraction as a function of pump torque for 0.7 ml/rev pump displacement and applied voltages from 12 to 28 volts in 4 volt increments. Results shown for tank precharges [depth limits] of 4.4 bar [30 m] and 7.6 bar [60 m].	19
Figure 5. Ballast tank vent operation time for 4.4 bar precharge pressure and vent valve nozzle area ratios from 5×10^{-5} to 3×10^{-4} in increments of 5×10^{-5}	20
Figure 6. Instantaneous system efficiency for pump displacement of 0.7 ml/rev, 4.4 bar precharge pressure, and various applied step voltages.	21
Figure 7. Instantaneous system efficiency for an applied voltage of 20 V, 4.4 bar precharge pressure, and various pump displacements.....	21
Figure 8. Ideal energy consumed per descend & ascend cycle per actuation water volume. VBS results shown for tank fill fractions from 0.5 to 0.9 in 0.1 increments.	25
Figure 9. Nondimensionalized energy storage device volume. VBS results shown for tank fill fraction of 0.9 and system efficiencies from 5 to 55% in 10% increments. CABS results shown for tank pressures limits of 150 to 350 bar in 50 bar increments.	26
Figure 10. Schematic of the ballast tank volume terms.	29
Figure 11. Relationship between neutral buoyancy volume, ballast tank volume, (a) max bidirectional actuation force, and (b) pressure ratio.	31
Figure 12. Notional vehicle setup with VBS. Schematic shown for (a) coordinate system, and (b) point mass/buoyancy approximations. All dimensions in mm, not drawn to scale. ..	33
Figure 13. Diagram for computing the viscous damping moment.	36

Figure 14. Vehicle and VBS actuator step response simulation. Step occurs at 0 s with step inputs shown in legend. All vehicle initial conditions set to zero. Step response results shown for (a) pitch, (b) depth, (c) tank 1 & 2 water volumes, and (d) motor 2 current..... 40

Figure 15. VBS Demo Platform prototype. 41

Figure 16. Elastic bladder inside ballast tank in (a) deflated and (b) inflated states. 43

Figure 17. Ballast tank design with precharge port 44

Figure 18. Descending maneuver at a nearly fixed pitch by pumping water into the fore and aft ballast tanks. 46

Figure 19. Pitch and depth change maneuver by venting the fore ballast tank..... 47

Figure 20. Extreme pitch maneuvers of (a) 83° pitch up and (b) -56° pitch down..... 47

Figure 21. Experimental and predicted (a) pitch response and (b) depth response to a forward ballast tank vent command initiated at $t = 0$ sec. 48

1. INTRODUCTION

The concept of a multi-domain unmanned vehicle that can travel through air, land, and/or sea domains is of great interest to the military, aerospace, and marine community. An airplane has unobstructed flight throughout the skies with high speed, high maneuverability, and high range capabilities. In contrast, a submarine has free range of the waters with high stealth and loitering capabilities. Combining these two vehicle concepts would produce a submersible aircraft capable of high speed and range through air as well as high stealth and persistence while underwater. A vehicle with these desirable capabilities would enable unique concept of operations that were previously impossible with a single-domain vehicle.

1.1. Brief Survey of Multi-Domain Vehicle Designs

The concept of a multi-domain vehicle has been around for decades. In the 1930s, the first manned flying submarine concept was proposed [1]. Since then there have been other attempts at manned aquatic-aerial domain vehicles but none of these prototypes demonstrated useful water and air operation [2]. The major design challenge was the added complexity from the vehicle being manned. Compared to an unmanned aquatic-aerial vehicle, a manned version must be significantly larger to fit a human crew and life support systems. A manned vehicle must also be structurally stronger to support the added loads from the crew, life support systems, and relatively larger payloads.

Much work has been done on aquatic-aerial unmanned vehicle designs. Most of these UAV designs can be categorized into three different types based on their method of launch and operation, which include seaplane taxiing, submarine-launched, or submersible [2]. The

seaplane UAV is capable of taking off and landing on the water surface through a conventional taxiing approach. Since this design is not capable of underwater operation, any loitering or surveillance must be performed while the vehicle floats on the water surface. Several seaplane UAV designs exist in the literature starting from 2002, such as the US NASA Ames Research Center's ACAT [3], the DRS RQ-15 Neptune [4], and the Warrior (Aero-Marine) Ltd.'s GULL24 and GULL36 [5]. The submarine-launched UAV has a much different concept of operations. The submarine-launched UAV is typically stored in the submarine torpedo tube while underwater. When deployed, the UAV is either launched by the torpedo tube or released and allowed to propel itself to the water surface. Upon breaking the water surface, many designs undergo some degree of morphing to enable aerial flight. For instance, the Sea Sentry [6] by Kollmorgen Corporation has forward and aft wing surfaces that are folded parallel to the fuselage while the UAV is stored in the submarine's universal modular mast (UMM). Upon breaking the water surface, the Sea Sentry's wings rotate 90° into a traditional fixed-wing configuration. Similarly, the Sea-Robin XFC [7] by the U.S. Navy features a pair of wing structures that are parallel to the fuselage while stored, then rotate into position when transitioning to air flight. Like the seaplane UAV, the submarine-launched UAV is not designed to operate underwater. It also requires a support vehicle like a submarine for underwater operation.

Compared to the previous two categories of aquatic-aerial vehicles, the submersible UAV design is the fullest-featured design. This UAV is capable of operating underwater, flying in the air, and transitioning between the two domains. Unlike the seaplane UAV, it is able to submerge and operate underwater and unlike the submarine-launched UAV, it does not need a

support vehicle while underwater. Much of the submersible UAV work in the literature feature bio-inspired designs. In 2009, Beihang University developed the Flying Fish [2], which was inspired by flying fish, waterfowls, and seaplanes. Their prototype vehicle is able to perform a seaplane taxiing takeoff from the water surface, fly in the air, and land again on the water surface via seaplane taxiing. The vehicle is also able to submerge by filling a ballast tank with the surrounding ambient water, then propel itself underwater using two water pumps. During submergence, the wings sweep back to become parallel to the fuselage to minimize drag. One of the key challenges with the submersible UAV is the water entry and water exit transitions. One studied water entry technique is the plunge dive, which is bio-inspired by the gannet. These birds have long slender bodies and wings that sweep back to minimize impact loads and increase their water penetration depths. They begin their dive from heights of up to 30 m in the air and plunge into the water at speeds of up to 24 m/s [8]. Several recent studies have been conducted on implementing the plunge dive into a submersible UAV design [9]–[11], but no prototype exists in the literature to date that demonstrates flight capabilities followed by a survivable plunge dive. The Naval Research Laboratory (NRL) also tested the plunge dive concept with their submersible UAV platform, Test Sub II [12]. Test Sub II demonstrated gliding aerial flight followed by a water landing via plunge dive or conventional skimming landing. The vehicle was not designed to submerge following a water landing, nor perform a takeoff from the water surface. Although the vehicle wings were not designed to sweep back during the plunge dive, the vehicle survived the plunge dive with minor structural damage.

For aquatic and terrestrial domain vehicle design, much of the recent work has focused on bio-inspired swimming/crawling robot designs [13]. The AmphiBot I and II are snake-like robots that use lateral body undulations for propulsion while in water and a crawling technique for locomotion on land [14], [15]. Similarly, the AmphiRobot I and II are also snake-like robots that use the same body undulation method for water propulsion, but instead use powered wheels while on land [16]. In addition to snake-like robots, legged amphibious robots designs have also been demonstrated. The AQUA is a robot with six appendages that is capable of both legged and swimming locomotion [17]. The six appendages function as legs for walking while on land and as paddles during swimming.

One of the major challenges of designing a multi-domain vehicle are the unusual vehicle operation requirements. The vehicle must have high durability to survive underwater environments and high reliability during domain transitions, yet be sufficiently lightweight and maneuverable such that air flight or land locomotion performance is minimally compromised. Many vehicle components or systems have primary functionality in only one domain, such as wings for air flight or wheels for land locomotion. While operating in the other domains, these inactive systems only increase the required vehicle size and weight, therefore decreasing the vehicle operating range and endurance. Thus, these single-function systems must be designed to meet the desired performance specifications with minimal impacts on the overall vehicle design while the system is inactive.

1.2. Buoyancy Control for UUVs

A variable buoyancy system (VBS) is a vehicle system functional in only one domain. This system is responsible for regulating the vehicle depth and orientation while operating underwater. In many unmanned underwater vehicles (UUVs), vehicle depth and orientation is exclusively controlled using the hydrodynamic forces over the vehicle's control surfaces [18]–[21]. Other UUV designs use thrusters to control vehicle depth and orientation [21], [22]. Depending on the payload weight, these vehicle designs are sometimes manually trimmed to near neutral buoyancy prior to the start of each mission. Trim techniques include adding weights or adjusting the amount of water in a ballast tank [23]. Similarly, UUV gliders use control surfaces and hydrodynamic forces for depth control but also internal actuators for attitude control. Gliders commonly control vehicle pitch by shifting an internal mass and therefore generating a restoring force due to the difference in center of gravity and center of buoyancy locations [24]. The SLOCUM glider [25] can also change the overall vehicle buoyancy during operation through the use of a thermal engine featuring internal and external bladders. Many UUVs feature an active buoyancy control system that adjusts the vehicle's total buoyancy throughout the mission [22], [23], [26], [27]. A variable buoyancy system (VBS) can also be used to exclusively control the vehicle's depth and orientation. This is advantageous for several reasons. First, there is no need for thrusters for depth or pitch control in the longitudinal plane. Second, depth or pitch regulation can be performed without any forward motion. UUVs that rely on control surfaces for depth and pitch control must have some forward velocity to generate hydrodynamic forces over the control surfaces.

Lastly, motionless loitering can be performed indefinitely with little to no energy input. Buoyancy control systems can also be found in nature. A sperm whale is able to control its net buoyancy through a large volume of spermaceti oil in the whale's head. The whale can heat or cool this oil by passing warm blood or cold seawater around it, causing the volume of oil to expand or contract slightly. As the volume of oil changes, so does the sperm whale's buoyancy [28].

Several methods of buoyancy control exist for underwater vehicles. Large manned submarines typically control the net vehicle buoyancy by using a ballast tank, the ambient water pressure, and compressed air. To decrease buoyancy and perform a dive maneuver, the flood valves of a ballast tank are opened and the ambient water pressure forces water into the tank. Simultaneously, any air inside the ballast tank is pushed out through a vent valve into the surrounding water, which prevents a buildup of air pressure inside the tank and enables the water to passively fill the ballast tank. With enough water in the ballast tank, the vehicle is able to reach neutral buoyancy. To perform an ascent maneuver, the flood valves are opened but the air vent valves are closed. Compressed air is then blown into the ballast tanks, forcing water out of the tank through the flood valves [29]. This buoyancy system design requires a second tank that stores the compressed air as well as an on-board air compressor to recharge the compressed air tank if the mission duration is long enough that the tank cannot store sufficient air. One potential drawback with this design is that the vehicle must access the water surface to operate the air compressor, which is undesirable if stealth is essential. Some unmanned UUVs similarly use the surrounding ambient water as the working fluid. These designs open flood valves and water passively fills the ballast tanks in order to

perform a dive maneuver [23], [27]. In some designs the air inside the tank is also vented as water is pumped in [27]. In contrast, other UUVs do not vent the air as water fills the vehicle and instead allow for a pressure buildup in the ballast tank or hull [30]. Other designs commonly use an active method of filling the ballast tank with the use of a water pump [22], [27], [30]. To increase buoyancy and perform an ascent maneuver, water is pumped out of the ballast tank. Instead of a rigid ballast tank, some UUVs also pump water into an elastic bladder that is located inside the vehicle hull [30].

Another buoyancy control approach is to use air as the working fluid. As part of the Test Sub II vehicle platform, Young [12] developed a buoyancy system featuring a forward and aft bladder system to control both depth and pitch. To increase buoyancy, air from the pressure hull is pumped into the bladders, increasing the bladder's volume and therefore the overall buoyancy. Air inside the bladders is then vented back into the pressure hull to decrease buoyancy. The major drawback with this design is that the system is inherently unstable in depth and heave velocity due to the compressibility of the working fluid, air. For instance if the bladders have a fixed amount of air contained in them and an environmental disturbance causes the vehicle to slightly increase depth, the increase in water pressure from the depth change causes the air inside the bladders to compress. As the bladder air is compressed, the volume displaced by the bladder decreases and so does the buoyancy force. To counter this instability, a closed-loop controller is required to maintain a reference depth or heave velocity input.

1.3. Proposed VBS Actuator

The VBS for a multi-domain vehicle has a special set of design requirements due to the vehicle's unique concept of operations. First, the VBS must be lightweight and compact in order to minimize the additional energy requirement for carrying the inactive VBS through the other domains. This includes minimizing the energy storage device volume, which may involve powering the VBS by the vehicle's existing energy source. Minimizing the VBS volume also frees up space for additional components such as sensors or payload, which may be useful in the air and land domains. Second, the VBS should be able to maintain the vehicle at a desired depth for loitering or surveillance operations. Lastly, the VBS should be able to perform extreme vehicle pitch angles that orient the vehicle horizontally or vertically. In a water-air domain vehicle, a horizontal orientation may be useful for efficient underwater locomotion or sensing while loitering. A vertical pitch-down maneuver could enable a streamlined heaving orientation for depth change via buoyancy control only. A vertical pitch-up maneuver could orient the underwater vehicle for an aerial vertical takeoff upon breaking the water surface. In a water-land domain vehicle, the same pitch-up maneuver could orient the vehicle for a water-land transition, such as a vertical wall climbing operation.

In this paper, we propose and investigate a VBS design suitable for multi-domain vehicles. The VBS design reflects multi-domain vehicle design objectives of high endurance, high stealth, and indefinite loitering capabilities. In Sec. 2 and 3, we develop and analyze a dynamic actuator system model for our VBS design. In Sec. 6 and 7, we develop a notional vehicle model and analyze the coupling between the VBS actuator and vehicle dynamics. In

Sec. 4, we compare the VBS design to a consumable compressed air buoyancy system in terms of energy per actuation and energy storage device volume. In Sec. 5, we discuss a methodology for sizing the VBS design based on the vehicle parameters. In Sec. 8, a proof-of-concept demonstration is presented and compared to the vehicle model-predicted results.

2. VARIABLE BUOYANCY SYSTEM MODEL

2.1. System Configuration

Ambient water from the surroundings is chosen as the VBS working fluid because of the ability to eject all working fluid prior to flight or land operations. Compared to VBS designs that use air and an on-board compressor, a water pump based VBS design does not need to resurface occasionally to recharge compressed air tanks. A VBS design that vents air also creates underwater air bubbles that are visible from the water surface especially in shallow waters, decreasing stealth. A rigid ballast tank concept was chosen to eliminate the system instabilities associated with using air and an external elastic bladder like in Young's design [12], which enhances loitering capabilities via less complicated controls and energy consumption. Furthermore, a battery powered VBS concept is chosen over a compressed air tank system due to electric batteries having a greater energy storage device density (see Sec. 4), resulting in a more compact VBS design.

Our proposed VBS ballast tank design consists of a rigid ballast tank with an inner elastic bladder to separate the air inside the tank from the working fluid (see Figure 1). To decrease net vehicle buoyancy or perform a dive maneuver, a positive displacement pump forces the

surrounding ambient water into the ballast tank and the elastic bladder, compressing the air inside the tank. A check valve downstream from the pump eliminates leakage through the pump due to backpressure. To increase vehicle buoyancy or perform an ascent maneuver, a proportional servo vent valve is opened and the water is forced out from the ballast tank due to the potential energy stored in the compressed air. The elastic bladder ensures that no air accidentally escapes during the venting operation regardless of the vehicle orientation.

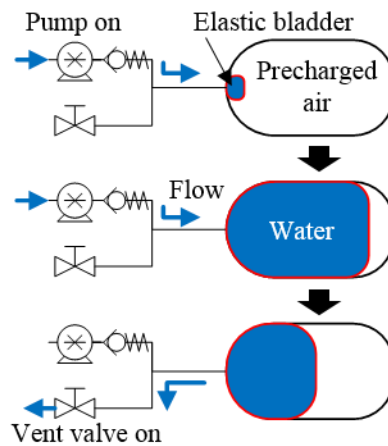


Figure 1. VBS ballast tank operating

Pre-pressurizing or precharging the air inside the tank is necessary so that the air pressure is always greater than the surrounding ambient water pressure, which is dependent on the vehicle's instantaneous depth. The vent valve operation relies on a positive pressure differential between the tank air pressure and the ambient water pressure in order to force the water out of the tank. The water pump and vent valve combination also requires less energy to operate than a VBS that exclusively uses a water pump. During a water vent operation,

powering a zero-power-hold on/off vent valve or a low power proportional solenoid vent valve uses less energy than powering a water pump to actively remove water from the tank.

2.2. Dynamic System Model

In order to investigate the relationship between control inputs and the VBS actuator force output, we begin by modeling the fluid dynamics for a single ballast tank. Due to the incompressibility of water, the system can be modeled using mass continuity and Bernoulli's equation for a streamline running from the pump outlet to inside the ballast tank. The dynamic hydraulic system equation is expressed as

$$P_o + \frac{\rho}{2} \left(\frac{\dot{V}_w}{A_p} \right)^2 = P_g \quad (1)$$

where P_o is fluid pressure at pump outlet, ρ is density of water, \dot{V}_w is the fluid's volumetric flow rate, A_p is cross-sectional area of the tubing at the pump outlet, and P_g and is pressure of the air inside the tank. Losses through the check valve, hydraulic tubing, and elastic bladder are assumed to be negligible. For the tubing and tank sizes used in the proof-of-concept prototype in Sec. 7, the tank fluid velocity is only about 0.2% of the tubing fluid velocity and therefore the tank fluid velocity is neglected. Assuming that the air compression process occurs over a relatively long period of time, the process can be approximated by the isothermal relation

$$P_g = \frac{P_{g,0} V_t}{V_t - V_w} \quad (2)$$

where $P_{g,0}$ is initial air pressure inside the tank, V_t is total volume of the ballast tank, and V_w is volume of water inside the tank. The initial air pressure inside the tank is function of the operation depth limit according to

$$P_{g,0} = \sigma(P_{atm} + \rho g Z_{max}) \quad (3)$$

where P_{atm} is atmospheric pressure, Z_{max} is the vehicle's operational depth limit, g is gravitational acceleration, and σ is a safety factor to ensure that the tank air pressure is always greater than the ambient water pressure.

The ballast tank and vent valve opening form a nozzle with an inlet and outlet area equal to the cross-sectional area of the tank and the cross-sectional area of the vent valve opening, respectively. The flow rate through this vent valve nozzle can also be modeled using mass continuity and Bernoulli's equation [8]. For a streamline running from inside the ballast tank to the vent valve outlet and taking positive flow to be into the tank, the fluid volumetric flow rate is expressed as

$$\dot{V}_w = -\kappa A_t \sqrt{\frac{2\eta(P_g - P_z)}{\rho(1 - \kappa^2)}} \quad (4)$$

$$\kappa = \frac{A_v}{A_t} \quad (5)$$

where η is nozzle efficiency, A_v is cross-sectional area of the vent valve opening, A_t is cross-sectional area of the ballast tank, and P_z is surrounding ambient water pressure. The ambient water pressure is equal to the pressure at the pump inlet and vent valve outlet. The nozzle area ratio, κ , is a control input through the use of a proportional servo valve.

The pump and motor system models are developed next. The required input torque for the constant displacement pump is expressed as

$$\tau = \frac{\delta(\Delta P)}{2\pi} \quad (6)$$

$$\Delta P = P_o - P_z = \frac{P_{g,0}V_t}{V_t - V_w} - \frac{\rho}{2} \left(\frac{\dot{V}_w}{A_p} \right)^2 - (P_{atm} + \rho g Z) \quad (7)$$

$$\dot{V}_w = \frac{\delta\omega\mu}{2\pi} \quad (8)$$

where δ is the pump's fixed volumetric displacement per revolution, Z is vehicle depth, \dot{V}_w is volumetric flow rate assuming a positive displacement pump, ω is pump shaft rotational speed, and μ is volumetric efficiency, which is a function of the pump outlet pressure [31]. The pump is assumed to be powered by a DC electric motor, whose dynamic model is expressed as

$$\dot{\omega} = \frac{K_e i - B_v \omega - \tau}{J} \quad (9)$$

$$\frac{di}{dt} = \frac{-iR - K_b \omega + E}{L} \quad (10)$$

where K_e and K_b are torque and speed constants, B_v is viscous damping coefficient, J is combined moment of inertia of motor armature and pump load, R is motor resistance, L is motor inductance, i is current, and E is applied voltage. The complete state equation for the volumetric flow rate is determined by combining (4) and (8) resulting in

$$\dot{V}_w = \frac{\delta\omega\mu}{2\pi} - \kappa A_t \sqrt{\frac{2\eta(P_g - P_z)}{\rho(1 - \kappa^2)}} \quad (11)$$

While the VBS is actuating, either the pump or the vent valve is operating; they will never be active simultaneously. Both the pump and vent valve can be inactive simultaneously, such as if the vehicle is loitering. Furthermore the pump can only operate in one direction such that $\omega \geq 0$. Thus the relation for water volumetric flow rate can be divided on the basis of three different operating conditions of applied voltage and vent valve ratio control inputs according to

$$\dot{V}_w = \begin{cases} 0 & \text{for } E = 0 \quad \kappa = 0 \\ \frac{\delta\omega\mu}{2\pi} & \text{for } E > 0 \quad \kappa = 0 \\ -\kappa A_t \sqrt{\frac{2\eta(P_g - P_z)}{\rho(1 - \kappa^2)}} & \text{for } E = 0 \quad \kappa > 0 \end{cases} \quad (12)$$

2.3. Variable Buoyancy System Actuator Analysis

With a dynamic system model for the VBS now defined, we consider modeling the actuation force, energy consumption, and system efficiency of the complete buoyancy system. The actuation force is dependent on the volume of the ballast tank and the water volume limit. If the same actuation force is desired in both the positive and negative heave directions, then the maximum bidirectional actuation force is expressed as

$$F_{max} = \frac{V_{w,max}}{2} \rho g \quad (13)$$

where $V_{w,max}$ is maximum water volume able to be pumped into the tank, which is limited by the pressure rating of the tank or the stall torque of the pump motor. When the vehicle is at neutral buoyancy, the ballast tank would have half its maximum water volume. The water volume limit is dependent on the motor and pump parameters, applied voltage, ballast tank

precharge, and tank volume. The water volume limit nondimensionalized by the ballast tank volume is determined by rearranging (6), (9), (11) and solving for the motor stall condition ($\dot{\theta} = 0$ and $i = V/R$) resulting in

$$\left(\frac{V_w}{V_t}\right)_{lim} = 1 - \frac{P_{g,0}}{\frac{2\pi K_e E}{R\delta} + P_{atm} + \rho g Z} \quad (14)$$

The instantaneous system efficiency during pump operation can be defined as the ratio of tank fluid output power to electrical input power as

$$\beta = \frac{P_{flow}}{P_{elec}} = \frac{\dot{V}_w(P_g - P_{atm})}{Ei} \quad (15)$$

The instantaneous system efficiency accounts for the losses in motor, pump, and hydraulic tubing network, although in this analysis we assume the pump and tubing losses to be negligible. The average system efficiency across the pump operating range is determined by integrating the instantaneous system efficiency with respect to tank fill fraction according to

$$\bar{\beta} = \frac{1}{h_{lim}} \int_0^{h_{lim}} \beta dh \quad (16)$$

$$h = \frac{V_w}{V_t} \quad (17)$$

The integral of P_{flow} with respect to time is equal to the fluid energy produced, W_{flow} . For comparison purposes, we consider the energy required to compress air, an ideal gas, from initial volume V_t to final volume $(V_t - V_w)$. Assuming an isothermal process, the energy required by the system to compress the air is expressed as

$$W_{gas} = -P_{g,0} V_t \ln \frac{V_t - V_w}{V_t} - P_{atm} V_w \quad (18)$$

When the hydraulic tubing losses are assumed to be negligible, $W_{gas} = W_{flow}$.

3. MODEL ANALYSIS RESULTS AND DISCUSSION

The VBS actuator model presented above is applied to a notional VBS actuator design. The motor parameters are for the Maxon brushed DC motor, model number 110124 [32]. The pump is assumed to be lossless and have an output pressure limited only by the stall torque of the motor. The baseline parameters for the system used throughout the parameter variation study are listed in Table 1. The ballast tank precharge pressure is directly related to the vehicle's depth limit by (3) and therefore the terms tank precharge pressure and depth limit are used interchangeably. All reported pressures are absolute units unless otherwise noted.

Table 1. Baseline parameters of the VBS Actuator

Parameter	Symbol	Value	Units
Tubing cross-sectional area	A_p	5.7	mm ²
Vent valve nozzle efficiency	η	0.9	Unitless
Motor and pump inertia	J	8.4	g cm ²
Motor inductance	L	0.89	mH
Motor resistance	R	13.8	Ω
Motor torque constant	K_e	17.1	mNm/A
Motor speed constant	K_b	558	rpm/V
Motor damping constant	B_v	2.49×10^{-7}	Nm.s/rad
Pre-pressurization safety factor	σ	1.1	Unitless

Figure 2 plots the maximum bidirectional actuation force as a function of ballast tank volume, vehicle depth limit, and tank pressure limit. The tank pressure limit is either the pressure rating of the tank or the maximum achievable pressure due to the pump motor stall characteristics. As the tank pressure limit increases for a fixed tank volume, the maximum actuation force increases since more water volume can be forced into the tank. The maximum actuation force shows decreasing sensitivity to the tank pressure limit as the limit is increased. This is because asymptotically increasing energy is required to compress the fixed mass of air inside the tank as its volume approaches zero. Maximum actuation force and vehicle depth limit are inversely proportional for a given ballast tank and tank pressure limit. Increasing the vehicle depth limit by increasing the tank precharge results in the pump motor reaching stall with less water inside the ballast tank, therefore decreasing the maximum actuation force.

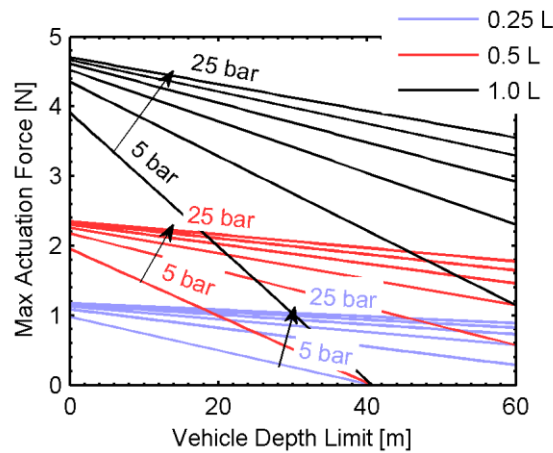


Figure 2. Maximum bidirectional actuation force as a function of vehicle depth limit for tank pressure limits from 5 to 25 bar in 4 bar increments.

Figure 3 plots the relationship between ballast tank fill fraction limit, precharge pressure, and applied voltage for a fixed pump displacement according to (14). The tank fill fraction limit dependence on depth is most prominent at lower voltages and higher tank precharges. Depending on the applied voltage and tank precharge, the ambient water pressure is nearly constant across the vehicle's operating depth range. In the remainder of this analysis, the ambient water pressure is assumed to be constant at atmospheric pressure in order to eliminate any required assumptions about the vehicle's depth change rate and instead focus the analysis on the actuator itself.

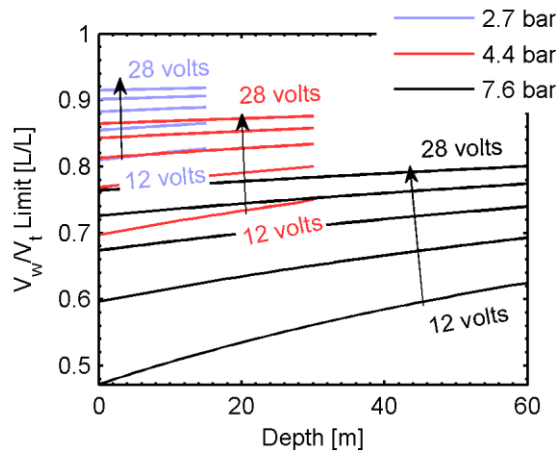


Figure 3. Ballast tank fill fraction limit as a function of vehicle depth for 0.7 ml/rev pump displacement and applied voltages from 12 to 28 volts in 4 volt increments. Results shown for tank precharges [depth limits] of 2.7 bar [15 m], 4.4 bar [30 m] and 7.6 bar [60 m].

During a system command to decrease net buoyancy, the control input to the VBS is the applied motor voltage. In Figure 4, we examine the relationship between applied voltage, pump torque, tank precharge pressure, and tank fill fraction. The pump torque is

nondimensionalized by the motor stall torque, which is dependent on the applied voltage. Increasing the tank precharge pressure shifts the tank fill fraction curves to the right because pump torque is proportional to precharge pressure according to (6).

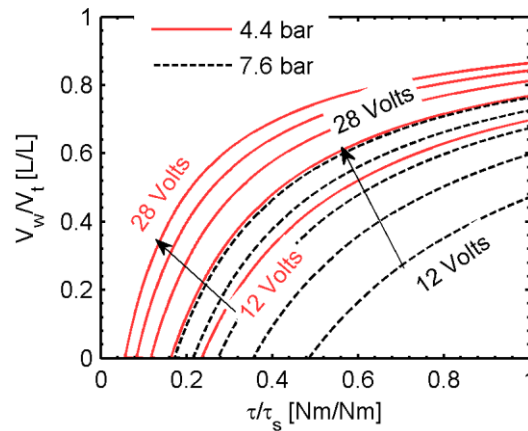


Figure 4. Ballast tank fill fraction as a function of pump torque for 0.7 ml/rev pump displacement and applied voltages from 12 to 28 volts in 4 volt increments. Results shown for tank precharges [depth limits] of 4.4 bar [30 m] and 7.6 bar [60 m].

During a system command to increase net buoyancy, the control input is the vent valve nozzle area ratio, κ . In Figure 5, we examine the effect of the nozzle area ratio on the rate of water exiting the ballast tank. The tank is assumed to have an initial fill fraction of 0.8 and a depth limit of 30 m. Next the vent valve is opened and the water is forced out of the tank by the internal compressed air. Tank emptying time shows decreasing sensitivity to nozzle area ratio as the ratio is increased. For instance, the decrease in emptying times from nozzle area ratio of 3.5×10^{-4} to 3×10^{-4} is minor compared to the decrease from 5×10^{-5} to 1×10^{-4} .

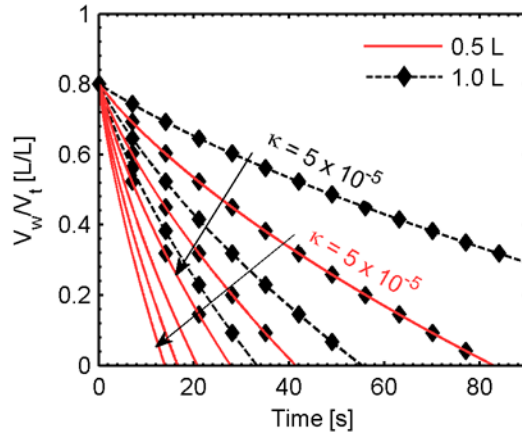


Figure 5. Ballast tank vent operation time for 4.4 bar precharge pressure and vent valve nozzle area ratios from 5×10^{-5} to 3×10^{-4} in increments of 5×10^{-5} .

The effect of applied voltage and pump displacement on system efficiency is plotted in Figure 6 and Figure 7. As applied voltage increases, instantaneous system efficiency increases across the tank fill fraction range because the motor is able to operate closer to its peak efficiency torque-speed operating point, which occurs at a high rotational speed. An optimal pump displacement is also apparent for maximum efficiency. For the range of pump displacements investigated, a pump displacement of 0.01 ml/rev is optimal if the tank is primarily operated between fill fractions of 0.4 – 0.8. This optimal pump displacement again corresponds to the motor operating most closely to its peak efficiency torque-speed operating point. As pump displacement is increased or decreased from this optimum, the motor speed is decreased or increased and the motor operates farther from its peak efficiency torque-speed operating point.

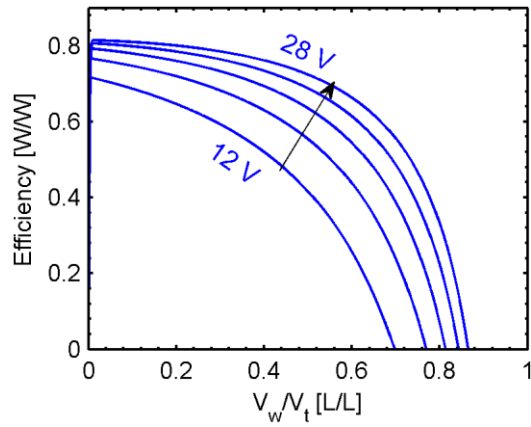


Figure 6. Instantaneous system efficiency for pump displacement of 0.7 ml/rev, 4.4 bar precharge pressure, and various applied step voltages.

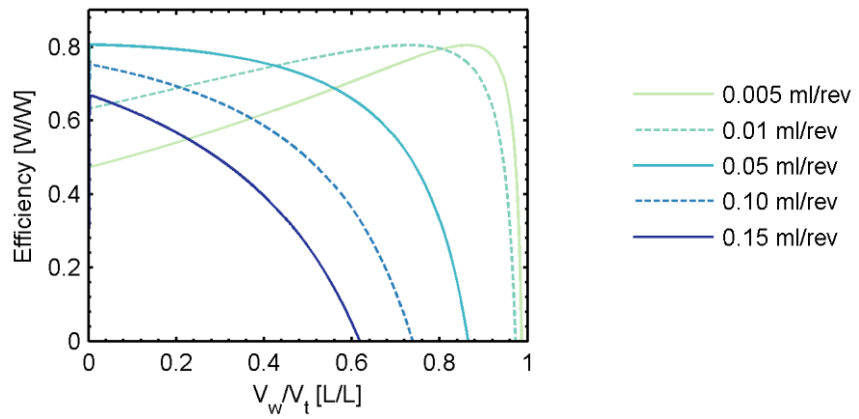


Figure 7. Instantaneous system efficiency for an applied voltage of 20 V, 4.4 bar precharge pressure, and various pump displacements.

4. COMPARISON TO CONSUMABLE COMPRESSED AIR BUOYANCY SYSTEM

For comparison purposes, we consider a consumable compressed air buoyancy system (CABS) in terms of energy storage device volume. Unlike the VBS which uses a battery as the main energy storage device, a CABS uses a tank of high pressure compressed air to convert the potential energy stored in the compressed air into mechanical work. In this analysis we consider each system to have the same ballast tank water volume limit and therefore the same maximum bidirectional actuation force. For the CABS, the water volume limit is equal to the ballast tank volume because the tank is able to be completely filled with water. This is not true for the VBS because the ballast tank volume is equal to the water volume limit plus a volume of captive air. The additional VBS ballast tank volume is expressed as $(V_t - V_{w,max})$ and is considered a part of the total VBS energy storage device volume because the captive air provides the energy for the venting operation. The VBS design uses one motor, pump, and vent valve per ballast tank while the CABS design uses three valves per ballast tank. These three valves include an air vent valve, a water flood valve, and a valve to the compressed air source. The volume of the VBS motor/pump combination is estimated to be roughly equivalent to the volume of the two extra CABS valves, resulting in both systems having comparable component volumes. Furthermore, both systems are approximated to only consume energy during either an ascent or descent cycle. The CABS only consumes compressed air energy during ascent maneuvers and although opening valves during the dive and ascent maneuvers require energy, this amount is assumed to be comparatively negligible. Similarly, the VBS only uses battery energy during dive

maneuvers and any energy consumed for valve actuation is assumed to be comparatively negligible.

To compare the energy storage device volumes of the VBS and CABS, we begin by determining the ideal energy consumption of the CABS to complete a specified descend/ascend cycle. We assume that the vehicle is initially on the water surface with the ballast tank empty. Next the vehicle fills the ballast tank to the water volume limit and begins the dive maneuver. Upon reaching the set cycle depth, the vehicle initiates the ascent maneuver by expelling all water from the tank and returns to the starting position at the water surface. The mass of compressed air required to expel all water from the ballast tank for the CABS as a function of depth can be determined from the ideal gas law according to

$$m_{air} = \frac{P_{g,0}V_t}{R_{air}T} \quad (19)$$

where R_{air} is the specific gas constant of air and T is the temperature of the air. This mass of air must be blown into the ballast tank to initiate every ascent cycle. The amount of energy in this mass of air available to do work is equal to $(P_{g,0} - P_{atm})V_t$. From the ideal gas law, the CABS compressed air tank volume is expressed as

$$V_{s,CABS} = \frac{Nm_{air}R_{air}T}{P_{CABS} - P_{g,0}} \quad (20)$$

where N the number of cycles and P_{CABS} is the pressure limit of the compressed air tank. At the end of the last cycle, the compressed air tank pressure is equal to the required ballast tank air pressure per cycle. Therefore at the start of the of the last cycle, a positive pressure differential always exists between the compressed air tank and ballast tank. The volume of

the VBS energy storage device is equal to the volume of the battery plus the volume of the additional ballast tank volume according to

$$V_{s,VBS} = \frac{NW_{gas}}{\bar{\beta}\epsilon} + V_t - V_{w,max} \quad (21)$$

where $\bar{\beta}$ is average system efficiency across the ballast tank fill fraction range and ϵ is battery volumetric energy density. The battery energy density was taken to be 1.2 MJ/L based on a survey of typical commercially available Li-Po batteries [33]. Figure 8 plots the ideal energy consumed per cycle comparison. It is expected that the CABS energy per cycle is lower because there is no asymptotic increase in ballast tank backpressure as the CABS blows air into the ballast tank. As the VBS ballast tank fill fraction approaches zero, the VBS curve approaches the CABS curve because the captive air backpressure is lower at smaller tank fill fractions. Figure 9 plots the energy storage device volume comparison for $N = 20$ and shows that depending on the compressed air tank pressure limit and the vehicle depth limit, even a relatively inefficient VBS is able to match the required energy storage device volume of the CABS. For instance, if the max pressure rating of the compressed air tank is 350 bar and the vehicle depth limit is greater than 30 m, then an overall VBS energy efficiency of only 15% is necessary for a smaller energy storage device volume compared to the compressed air tank of the CABS. From Figure 6, Figure 7, and (16), average system efficiencies of up to 72% are possible depending on the motor, pump displacement, and applied voltage. Furthermore, a max pressure rating of 350 bar is on the high end for lightweight, commercially available compressed air tanks. Table 2 lists typical specifications for a few different types of commercially available compressed air tanks.

Table 2. Typical commercially available compressed air tank specifications

Tank Type	Volume [L]	Weight [kg]	Pressure [bar]
Paintball compressed air tank, carbon fiber [34]	0.7 – 1.5	0.80 – 1.3	207 – 310
Scuba diving tank, aluminum [35]	0.9 – 13.2	1.2 – 18.6	207 – 228
Scuba diving tank, composite [35]	11.1	15.3	300

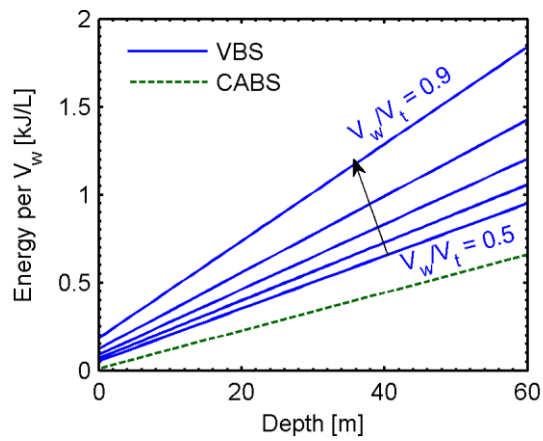


Figure 8. Ideal energy consumed per descend & ascend cycle per actuation water volume. VBS results shown for tank fill fractions from 0.5 to 0.9 in 0.1 increments.

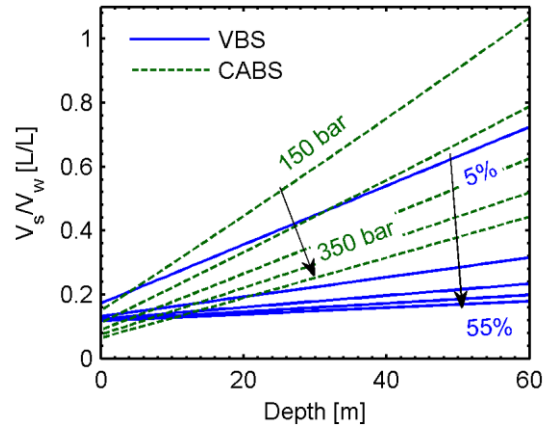


Figure 9. Nondimensionalized energy storage device volume. VBS results shown for tank fill fraction of 0.9 and system efficiencies from 5 to 55% in 10% increments. CABS results shown for tank pressures limits of 150 to 350 bar in 50 bar increments.

5. HOW TO SIZE THE BALLAST TANK

This section presents a methodology on how to design the VBS ballast tank. This methodology is for a single ballast tank but can be extended to include multiple tanks. The procedure is also for obtaining an equal bidirectional actuation force but can be modified if different actuation forces are desired for the positive and negative heave directions. To begin sizing the ballast tank, we first consider the vehicle parameters prior to adding the VBS system. To bring the vehicle to neutral buoyancy, the VBS must offset the vehicle's existing buoyancy force resulting in zero net force acting on the vehicle. The net force acting on the vehicle with the VBS is determined by

$$F_{net} = W_0 + W_{VBS} + \rho V_w g - (B_0 + B_{VBS} + B_t) \quad (22)$$

where W_0 and B_0 is the total vehicle weight and buoyancy prior to adding the VBS and W_{VBS} is the total dry weight of the VBS which includes the weight of the tank, motor, pump, valves, ballast tank, hydraulic plumbing, and additional components. The buoyancy force from the external VBS ballast tank is B_t and the buoyancy force from any additional external VBS components is B_{VBS} . If the ballast tank and any additional VBS components are packaged inside the existing vehicle hull or dry payload bay, then B_t and B_{VBS} would be zero. The ballast tank buoyancy force is related to the ballast tank size by the relationship $B_t = \rho V_t g$, where V_t is the volume of the ballast tank. Equation (22) shows that if the ballast tank is empty of water and if the sum of the total VBS buoyancy force and total dry weight is positive ($B_{VBS} + B_t + W_{VBS} > 0$), then the sum of the initial vehicle buoyancy force and total dry weight must be negative ($B_0 + W_0 < 0$). In other words, the net buoyancy of the vehicle prior to adding the VBS must be negative if the net buoyancy of the VBS addition is positive. If the VBS is added externally to the existing vehicle, then the buoyancy contributions of the VBS ballast tank and additional components can be rewritten in terms of water displacement volumes and grouped into a single water volume displacement term resulting in

$$V_{0,NB} = V_t - V_w + V_{VBS} \quad (23)$$

where V_{VBS} is the volume of the VBS components not packaged inside the existing vehicle. The term $V_{0,NB}$ represents the volume of water displacement required to bring the existing vehicle with no VBS to neutral buoyancy. To determine $V_{0,NB}$ based on vehicle parameters, we multiply both sides of equation (23) by ρg to turn the volumes into buoyancy forces, substitute the result into equation (22), and set $F_{net} = 0$, resulting in

$$V_{0,NB} = \frac{W_0 + W_{VBS} - B_0}{\rho g} \quad (24)$$

Thus the required volume of water displacement from the VBS is dependent on the initial dry weight of the vehicle, weight of the VBS, and the initial buoyancy force of the vehicle. To study the relationship between $V_{0,NB}$ and the size of the ballast tank we examine the case where V_{VBS} is negligible, resulting in $V_{0,NB} = V_t - V_w$. Another constraint on this ballast tank sizing procedure is that an equal bidirectional actuation force is desired in both the positive and negative heave directions. As a result the ballast tank must be sized such that neutral buoyancy is achieved when the tank is filled to half of its water volume limit, or $V_w = V_{w,max}/2$. When the water volume limit is present inside the ballast tank, the volume of captive air is at its minimum. This air volume is determined by the isothermal gas compression assumption according to

$$V_{g,f} = \frac{P_{g,0}V_t}{P_{g,f}} \quad (25)$$

where $P_{g,f}$ is the tank pressure limit. The water volume limit able to be pumped into the tank must be determined when the vehicle is at zero depth. If the water volume limit was determined when the vehicle was at a specific depth, then the resulting maximum actuation force could only be reached at that specific depth due to the ambient water pressure aiding the motor and pump. With these constraints, the volume of water displacement required to bring the existing vehicle to neutral buoyancy can be now determined. Figure 10 shows a schematic of the ballast tank at neutral buoyancy with the previously defined volume terms.

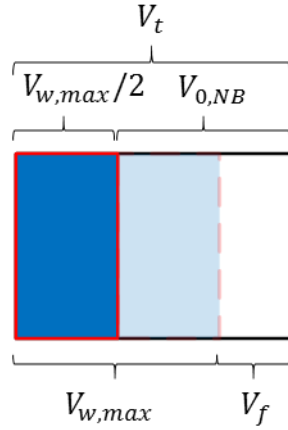


Figure 10. Schematic of the ballast tank volume terms.

The size of the ballast tank can be modeled as a function of the water volume limit and minimum captive air volume according to equation (25), resulting in

$$V_t = V_{w,max} + \frac{P_{g,0}V_t}{P_{g,f}} \quad (26)$$

Thus, the ballast tank size is a function of the water volume limit, initial precharge pressure, and the tank pressure limit. Due to the desired equal bidirectional actuation force constraint, another ballast tank sizing relationship shown in Figure 10 is

$$V_{0,NB} = \frac{V_{w,max}}{2} + \frac{P_{g,0}V_t}{P_{g,f}} \quad (27)$$

Equations (26) and (27) form a system of equations that describe the required ballast tank size. For this tank sizing design problem, it is more convenient to investigate the max bidirectional actuation force rather than the max water volume. After replacing $V_{w,max}$ with F_{max} according to equation (13), the new system of equations describing the required ballast tank size is

$$V_t = \frac{2F_{max}}{\rho g} + \frac{P_{g,0}V_t}{P_{g,f}}$$

$$V_{0,NB} = \frac{F_{max}}{\rho g} + \frac{P_{g,0}V_t}{P_{g,f}} \quad (28)$$

$V_{0,NB}$ is a known parameter based on the vehicle parameters. From the solution to the system of equations, the max bidirectional actuation force can be expressed as a function of the ballast tank size and $V_{0,NB}$ according to

$$F_{max} = \rho g(V_t - V_{0,NB}) \quad (29)$$

This equation is independent of the pressure ratio. Therefore if two of the design parameters ($F_{max}, V_t, V_{0,NB}$) are known or selected, then the third parameter is automatically determined. Based on the constraint that V_{VBS} is negligible, the tank volume is constrained to be greater than or equal to the neutral buoyancy volume ($V_t > V_{0,NB}$). The neutral buoyancy volume must also be greater than half of the tank volume, or ($V_t < 2V_{0,NB}$), based on the constraint for an equal bidirectional actuation force. If the latter equality is violated, then the vehicle would not be at neutral buoyancy when $V_w = V_{w,max}/2$ based on Figure 10. For any valid combination of $F_{max}, V_t,$ and $V_{0,NB}$ that satisfies equation (29) or shown in Figure 11(a), a specific pressure ratio is required based on the system of equations in (28). Figure 11(b) plots the required pressure ratio as a function of the neutral buoyancy volume and ballast tank volume.

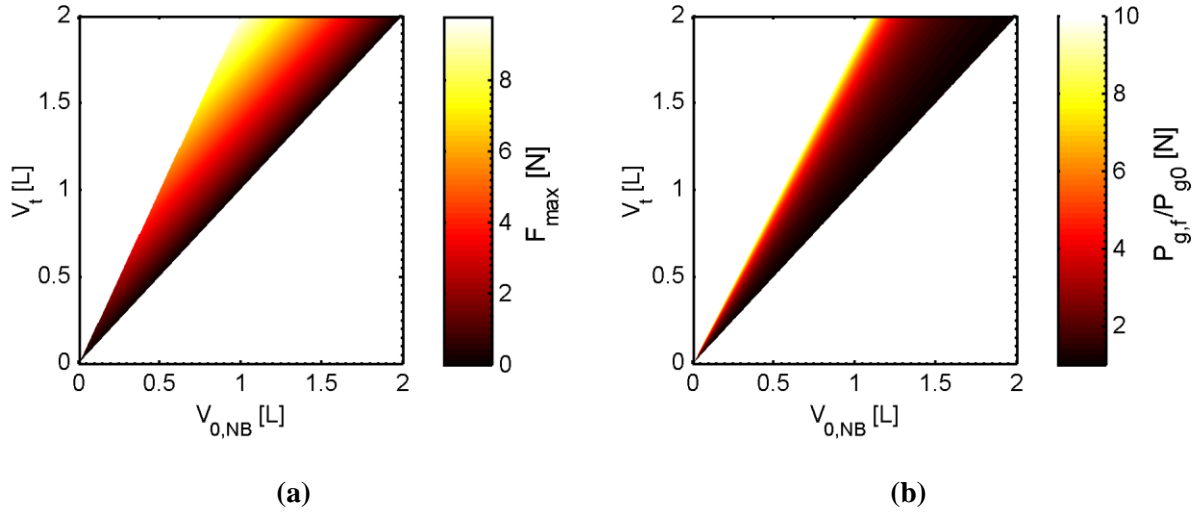


Figure 11. Relationship between neutral buoyancy volume, ballast tank volume, (a) max bidirectional actuation force, and (b) pressure ratio.

A $P_{g,f}/P_{g,0}$ pressure ratio of unity means that the max achievable tank pressure is equal to the initial precharge pressure. As a result, no water can be pumped into the tank and therefore the max actuation force is zero. For this special case the required ballast tank size is simply equal to the required water displacement volume for neutral buoyancy. As the pressure ratio increases from unity, asymptotic behavior is observed in Figure 11(b) as the constraint $V_t < 2V_{0,NB}$ is approached. This is due to the asymptotically increasing energy required for compressing the air inside the ballast tank as the air volume approaches zero.

From Figure 11, the complete relationship between neutral buoyancy volume, ballast tank volume, max actuation force, and pressure ratio can be determined. For instance, for a specific $V_{0,NB}$ based on vehicle parameters and desired F_{max} , the required tank volume and required pressure ratio can be determined. Or, for a specific $V_{0,NB}$ and selected pressure ratio, the required tank volume and max actuation force can be determined. A design tradeoff must

be made between tank size and max actuation force. Minimizing the ballast tank volume has the advantage of minimizing the required pressure ratio, reducing the pressure loads on the ballast tank resulting in a more lightweight and compact ballast tank. However, minimizing the tank size limits the max actuation force, resulting in limited vehicle depth and pitch control rates. On the other hand, maximizing the max actuation force results in a larger required tank size and higher required pressure ratio. A high pressure ratio means high pressure loads on the ballast tank, resulting in an undesirable heavier ballast tank design due to the large structural loads.

6. DYNAMIC VEHICLE SYSTEM MODEL

6.1. System Configuration

To examine the coupling between the VBS actuator and vehicle dynamics, a notional underwater vehicle is modeled. The simplified vehicle model consists of two VBS actuators located forward and aft to enable depth and pitch control. For modeling purposes each set of motor, pump, and vent valve assembly are lumped into single point masses and point buoyancies. The complete vehicle is then modeled as a system of six point masses and six point buoyancies. The point buoyancy location for each component is assumed to be coincident with the point mass location at the centroid. The vehicle is represented schematically in Figure 12. Table 3 lists the mass and buoyancy values for each component.

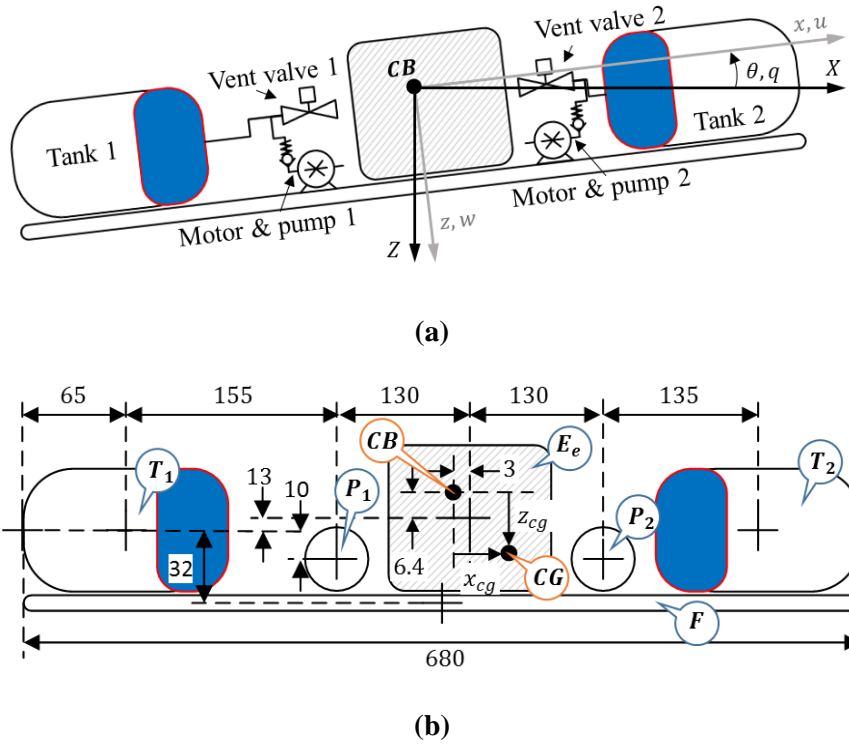


Figure 12. Notional vehicle setup with VBS. Schematic shown for (a) coordinate system, and (b) point mass/buoyancy approximations. All dimensions in mm, not drawn to scale.

Table 3. VBS Test Platform II component approximations

Component	Symbol	Mass [kg]	Buoyancy [N]
Ballast tank 1, dry	T_1	0.065	2.45
Ballast tank 2, dry	T_2	0.065	2.45
Motor, pump, valve assembly 1	P_1	0.380	1.02
Motor, pump, valve assembly 2	P_2	0.380	1.02
Electronics enclosure	E_e	0.650	10.3
Structural frame	F	0.025	0.0583

The vehicle's center of buoyancy (CB) location is determined by a buoyancy force balance in the x and z directions according to

$$x_{cb} = \frac{V_1 x_1 + V_2 x_2 + \dots + V_n x_n}{V_1 + V_2 + \dots + V_n} \quad (30)$$

where V_n and x_n is water displacing volume and x -location of the n th component relative to the trailing edge of the aft ballast tank. The same procedure is used to determine the CB z -location. The vehicle CB location is fixed and therefore the body-fixed coordinate system origin is chosen to be coincident with the CB. The vehicle center of gravity (CG) is determined by a force balance according to

$$x_{cg} = \frac{x_1(m_1 + \rho V_{w,1}) + x_2(m_2 + \rho V_{w,2}) + m_3 x_3 + \dots + m_n x_n}{m_1 + \rho V_{w,1} + m_2 + \rho V_{w,2} + m_3 + \dots + m_n} \quad (31)$$

where m_n and x_n are mass and x -location of the n th component relative to the CB and $\rho V_{w,n}$ is the mass of the water in the n th ballast tank. The mass of water in each tank is modeled as coincident with the ballast tank point mass locations.

6.2. Nonlinear System Model

Throughout the literature [36]–[38], generalized underwater vehicle's dynamic equations of motion can be described by

$$\mathbf{M}\dot{\underline{v}} + \mathbf{C}\underline{v} + \mathbf{D}\underline{v} + \underline{G} = \underline{\tau}_f \quad (32)$$

where \mathbf{M} is sum of the inertia and added mass matrices, \mathbf{C} is sum of the rigid-body and hydrodynamic Coriolis and centripetal matrices, \mathbf{D} is damping matrix, \underline{G} is restoring force vector, and $\underline{\tau}_f$ is vector of external forces and moments. For a vehicle controlled exclusively

by varying its buoyancy and assuming no water currents, the external force vector is zero. Considering only motion in the longitudinal plane, the velocity and position vectors reduce to

$$\underline{v} = [u, w, q]^T \quad (33)$$

$$\underline{\eta} = [X, Z, \theta]^T \quad (34)$$

where \underline{v} is expressed with coordinates in the body-fixed frame and $\underline{\eta}$ is expressed with coordinates in the earth-fixed frame (see Figure 12).

To estimate the added mass and damping terms, the vehicle shape was approximated as a prolate ellipsoid whose major and minor axes correspond to the vehicle's length ($l = 0.68$ m) and width ($d = 0.1$ m), respectively. The rigid-body inertia matrix is modeled from rigid-body Newton-Euler equations and is dependent on the vehicle's total mass, moment of inertia, and CG location [37], [38]. For a vehicle with three planes of body symmetry and operating at low speeds, the added mass matrix is simplified to a diagonal structure [36], [37]. The added mass terms for a prolate ellipsoid are described by Fossen [37].

The normal and axial force coefficients are described by Jorgensen [39] as

$$C_N = \frac{A_p}{A_r} C_{d_n} \sin^2 \alpha \quad (35)$$

$$C_A = C_{A_o} \cos^2 \alpha \quad (36)$$

where α is the angle of attack, A_p is the planform area, A_r is the reference area, C_{d_n} is the crossflow drag coefficient ($C_{d_n} \approx 1.2, Re < 3 \times 10^5$ [39]), and C_{A_o} is the axial drag coefficient at zero angle of attack ($C_{A_o} = 0.25$ [40]). For a vehicle traveling at speed U , the normal and axial forces are

$$F_N = \frac{C_N \rho U^2 A_r}{2} \quad (37)$$

$$F_A = \frac{C_A \rho U^2 A_r}{2} \quad (38)$$

The viscous damping moment is calculated by integrating the damping force on a differential area of the ellipsoid (see Figure 13) at a position $(a - 1)l \leq r \leq al$ relative to the CG location along the major axis according to

$$M_q = \frac{1}{2} \rho C_{D,q} \int_{(a-1)l}^{al} d_d |v| v r dr \quad (39)$$

where the upper and lower limits of integration represent the leading and trailing edges of the ellipsoid along its major axis [41].

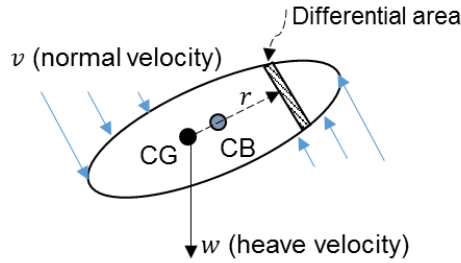


Figure 13. Diagram for computing the viscous damping moment.

Based on drag coefficients for two-dimensional circular bodies given by Cengel and Cimbala [40], $C_{D,q}$ is 1.2. The CG location along the ellipsoid major axis is located a distance al from the trailing edge, where a is a dimensionless parameter such that $a = 1$ corresponds to the leading edge, and $a = 0$ corresponds to the trailing edge. The variable v is the local velocity component normal to the ellipsoid body and is a function of the distance from the CG as

$$v = -w + (r + x_{cg})q \quad (40)$$

where w and x_{cg} are defined with respect to the CB x-location and r is with respect to the CG x-location. The variable d_d is the width of the differential segment and is a function of the location along the ellipsoid's major axis according to

$$d_d = d \sqrt{\left|1 - \left(\frac{2r}{l}\right)^2\right|} \quad (41)$$

The restoring force vector is expressed as

$$\underline{G} = \begin{bmatrix} (W - B)\sin(\theta) \\ -(W - B)\cos(\theta) \\ (z_{cg}W - z_{cb}B)\sin(\theta) + (x_{cg}W - x_{cb}B)\cos(\theta) \end{bmatrix} \quad (42)$$

where W is total weight of the vehicle and B is total buoyancy force. The VBS actuator and vehicle dynamics are coupled through the mass matrix and CG terms x_{cg} and z_{cg} . The vehicle nonlinear dynamics are then expressed as

$$\begin{bmatrix} \dot{u} \\ \dot{w} \\ \dot{q} \end{bmatrix} = -\mathbf{M}^{-1}\mathbf{C} \begin{bmatrix} u \\ w \\ q \end{bmatrix} - \mathbf{M}^{-1} \begin{bmatrix} F_A \\ F_N \\ M_q \end{bmatrix} - \mathbf{M}^{-1}\underline{G} \quad (43)$$

$$\dot{X} = u \cos \theta + w \sin \theta \quad (44)$$

$$\dot{Z} = -u \sin \theta + w \cos \theta \quad (45)$$

$$\dot{\theta} = q \quad (46)$$

7. VEHICLE SYSTEM DYNAMIC RESULTS

Figure 14 plots the vehicle response to different VBS actuator step inputs. The vehicle is initially motionless, neutrally buoyant, and fully submerged near the water surface, with an

initial pitch angle of -7.6° . This pitch angle corresponds to the statically stable orientation of the vehicle due to the difference in the initial CG and CB locations. Both ballast tanks have an initial ballast tank fill fraction of 0.4. Each tank has a precharge pressure of 4.4 bar and therefore the vehicle depth limit is 30 m. The first step response, shown in blue, represents a pitch change only maneuver. A 18 V step input is sent to the forward pump motor and a step input of $\kappa = 7.8 \times 10^{-5}$ is sent to the aft vent valve, causing the CG to shift forward and the vehicle to pitch downward. Once the motor has reached the stall current, the applied voltage is removed and the current goes to zero. The steady-state value of the ballast tank water volumes shows the tank 1 fill fraction limit is 0.8 while the tank 2 fill fraction is zero, resulting in the vehicle being neutrally buoyant and the net force on the vehicle in the heave direction to be zero. During the transient response of the ballast tank water volumes, the water flow rates for tank 1 and 2 are slightly different and therefore the vehicle is not neutrally buoyant at all times. As a result, the vehicle depth fluctuates slightly about zero in Figure 14(b). The second step response, shown in black, represents a pitch and depth change maneuver. The only input is a 12 V step input to the forward pump motor. The water level in tank 1 remains constant throughout the simulation. In comparison to the pitch change only maneuver, the magnitude of the steady-state vehicle pitch result is much smaller. This is expected because not emptying the water from tank 1 results in the CG shifting less forward. The third step response, shown in red, represents a depth change only maneuver. Both pump motors receive a 14 V step input and thus the forward and aft ballast tanks fill with water at the same rate. The steady-state pitch response is not zero because the two ballast tanks are not equidistant from the center of rotation. One interesting result is that although the second

step response pumps water into the ballast tank(s) at a slower rate than in the third step response, the second step response achieves a faster heave velocity. The pitch change in the second step response orients the vehicle into a more streamlined position for heaving with less drag. The implication from this result is that a vehicle energy efficiency advantage exists with extreme pitch control. In the second response, only one motor is active and operated at a lower voltage and current, resulting in a much lower system energy consumption than in the third response.

The step response results show the vehicle stability with the presented VBS actuator design. For all three initial step inputs, the vehicle reaches a stable, constant terminal velocity. This is in contrast to a VBS design using an external air bladder, which does not reach a stable vehicle velocity in response to a step input. This inherent stability reduces the complexity of adding a controller if an autopilot or closed-loop depth and pitch regulation is desired.

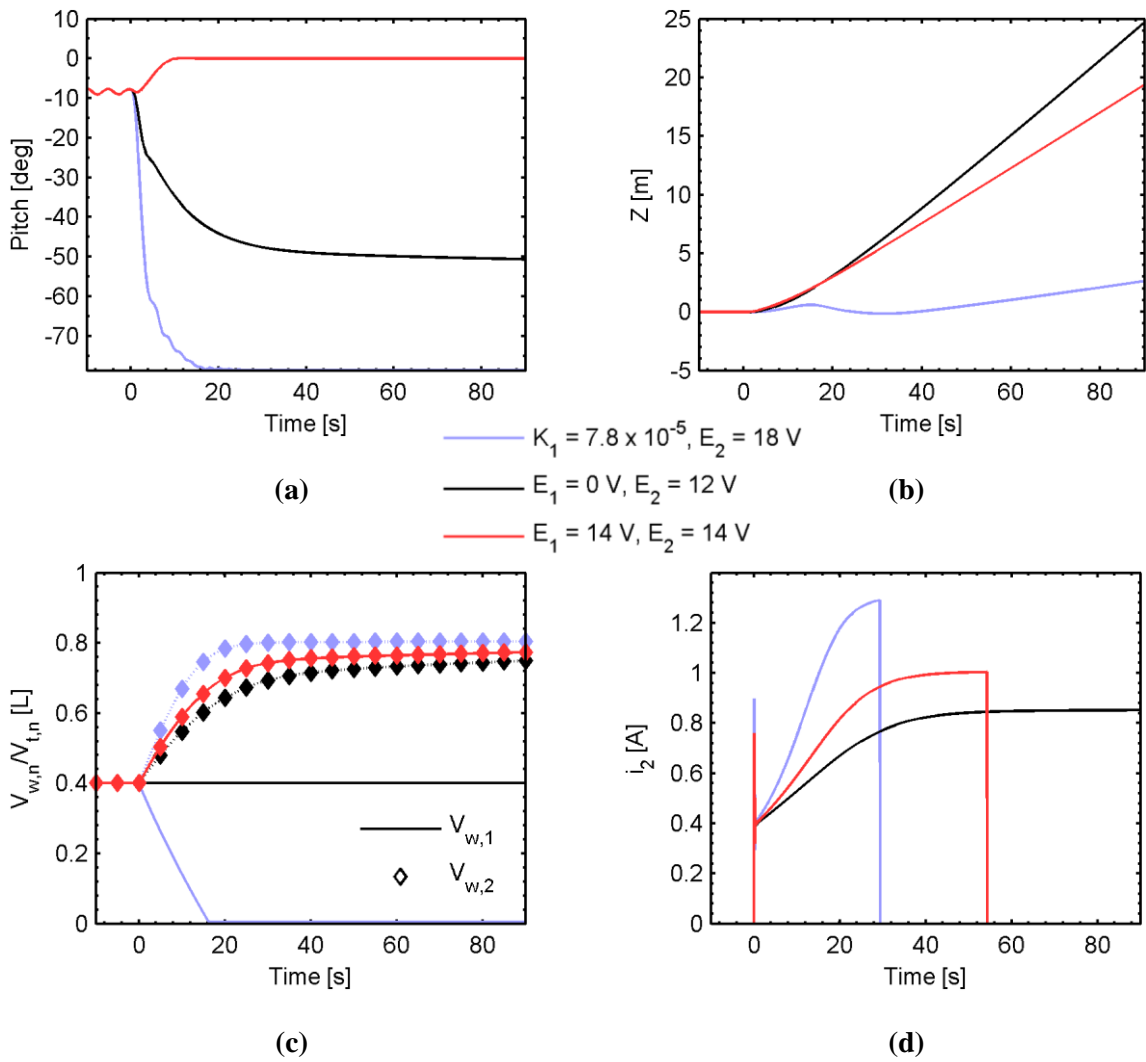


Figure 14. Vehicle and VBS actuator step response simulation. Step occurs at 0 s with step inputs shown in legend. All vehicle initial conditions set to zero. Step response results shown for (a) pitch, (b) depth, (c) tank 1 & 2 water volumes, and (d) motor 2 current.

8. PROOF-OF-CONCEPT DEMONSTRATION

The VBS Demo Platform proof-of-concept was constructed to demonstrate the VBS actuator design and vehicle depth and pitch control (see Figure 15). The overall vehicle length is 0.64 m and the max body width is 0.1 m. The total dry mass is 1.3 kg and the total buoyancy is 16.7 N. The vehicle features two ballast tanks and a single motor and pump combination. The hydraulic tubing cross-sectional area is the same as that listed in Table 1. The volume of each ballast tank is 250 ml. The motor is powered by a 3 cell Li-Po, 2100 mAh battery and is controlled through a radio transmitter operating at 72 Mhz.

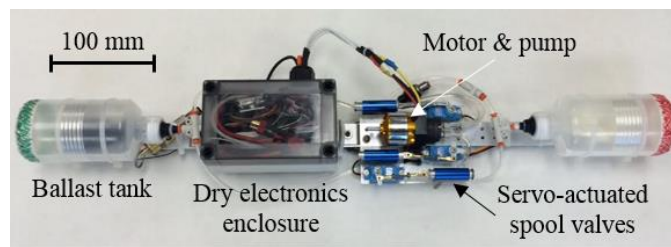


Figure 15. VBS Demo Platform prototype.

The motor and pump are hobby RC components intended for hydraulic oil applications. The motor is a brushless DC motor connected to a 50 A electronic speed controller (ESC). The pump is a mini hydraulic oil pump intended for use with hobby RC oil hydraulic actuators and has a max pressure specification of 80 bar. For oil pumps of this scale, 80 bar is very high and therefore questionable because of its low cost design. However, since the max operating pressures in our application are only about 8 bar, no testing of the pump's claimed max pressure was necessary. There were no noticeable performance issues when using water

instead of hydraulic fluid during operation. Nonetheless, it is important that the pump is cycled using hydraulic oil following any operation with water to force any residual water out of the pump chambers. If any residual water is allowed to sit for even just a few hours, the working fluid is noticeable rust-filled during the next operation. One somewhat unexpected result is that the motor and pump are able to operate underwater with no additional waterproofing needed. One caveat is that if the motors are not completely dried or sprayed with WD-40 following submergence testing, the residual water can cause minor rusting on the bearing sleeves and races. This rust has not caused any noticeable performance issues to date.

A servo-actuated spool valve assembly directs which tank is connected to the pump and therefore only one tank can be pumped at a time. Each tank is connected to its own vent valve, which consists of another servo-actuated spool valve assembly. The waterproof servos used are the Hi-Tec HS-5086WP. Compared to traditional non-waterproof servos, the selection of COTS waterproof servos is limited. Waterproofing techniques exist for traditional COTS non-waterproof servos, which increases the selection of servos to choose from. Ultimately for our application the COTS waterproof servos met our specifications and eliminated the hassles associated with servo waterproofing. The servos were connected to the wiring setup using the Molex Mizu-P25 lineup of waterproof electrical connectors.

The battery, RC receiver, and ESC are all stored inside the watertight electrical enclosure. The electrical wires exit the watertight enclosure through a standard watertight cord grip. The antenna wire of the RC receiver is also passed through the cord grip and run along the body of the vehicle. Noticeable cross-talk issues and decreased communication distances occurred

if the antenna wire was kept inside the electrical enclosure. A 2.4 GHz transmitter and receiver were also tested, but communication was unsuccessful when submerged under a couple feet of water. The higher frequency signal experienced much greater attenuation by the water than 72 MHz.

Each ballast tank is a 250 ml HDPE lab bottle and although these bottles are not designed to hold pressure, burst tests experiments showed that they could withstand pressures up to 100 – 120 psi, which is more than sufficient for our proof-of-concept vehicle. Burst tests also showed that the failure mode is typically due to material elongation followed by rupture along the flash lines from the blow molding process. In an effort to increase the burst pressure of the bottles, fiber reinforced strapping tape is wrapped around the bottle diameter. However, no further burst test experiments were conducted to test the new burst pressure of the reinforced bottles. A pressure relief valve is also connected to each ballast tank to reduce the likelihood of bursting. The elastic bladder inside the ballast tank is a high-quality latex balloon. Figure 16 shows the bladder in its deflated and inflated states.



Figure 16. Elastic bladder inside ballast tank in (a) deflated and (b) inflated states.

For the VBS Demo Platform, precharging the captive air inside the ballast tanks was unnecessary because the max vehicle depth was only 11 ft, which was the max depth of the pool used for testing. Ballast tank designs with the ability to add precharge were also investigated and shown in Figure 17. A second thru-wall fitting is installed in the tank and acts as the precharge port. A check valve on the precharge port ensures that the precharge pressure cannot escape. To vent the precharge pressure, either the check valve is removed or the bottle cap is loosened. Although a globe or ball valve in place of the check valve would enable easier precharge venting, a check valve was chosen due to the weight advantage and because the need to vent the precharge pressure was uncommon.

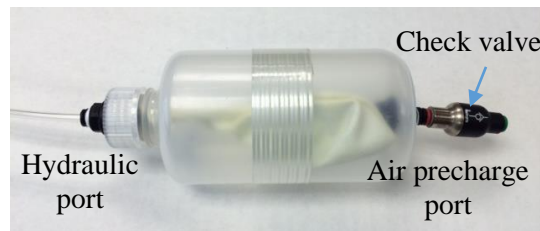


Figure 17. Ballast tank design with precharge port

One issue during operation is the presence of air in the hydraulic lines and bladder. Upon initially placing the dry vehicle in water and running the VBS to perform a dive maneuver, the residual air that is present in the hydraulic lines and bladder becomes trapped by the incoming pumped water. This is an inherent issue for any VBS system that uses pumps and water as the working fluid. However, initially running the VBS through a series of pumping and venting cycles mitigates this issue. In our experiments, one or two pumping and venting

cycles was sufficient to bleed the air from the hydraulic lines, as evidenced by the disappearance of air bubbles during venting cycles.

Proof-of-concept testing was performed at the Carmichael Aquatic Center at North Carolina State University. The vehicle was manually controlled with an RC transmitter. With human-in-the-loop control, the vehicle demonstrated maneuvers including pitch control, depth regulation at a fixed pitch, and loitering at a constant depth. A waterproof HD video camera operating at 60 frames per second was mounted to the pool floor and used to record the vehicle location and orientation during testing. The videos were post-processed frame by frame to determine the vehicle depth and pitch angle as functions of time. Figure 18 and Figure 19 show video frames from a nearly fixed-pitch depth change maneuver and a pitch and depth change maneuver, respectively. The vehicle is able to descend while remaining approximately horizontally pitched by running the motor steady and frequently diverting the flow from one ballast tank to the other. For the pitch and depth change maneuver in Figure 19, the vehicle was initially loitering at a constant depth at neutral buoyancy. The vent valve on the fore ballast tank was then opened, causing the vehicle to pitch up and start ascending. Figure 20 shows the extreme pitch angle capabilities of the vehicle.

The analytical model presented in the preceding section was applied to match the parameters of the VBS Demo Platform and three unknown parameters were empirically determined for the experiment apparatus. The ballast tank water volumes required for neutral buoyancy at near-zero pitch angle were first experimentally determined. For this near-zero pitch configuration, the vehicle CG and CB locations were then estimated from static force balance experiments. The CG and CB location estimates were then refined by fitting the

model-predicted results to the experimental results, which are shown in Figure 21. Likewise, the vent valve nozzle efficiency parameter was determined by fitting the model-predicted results to the experimental results, resulting in a value of 0.10. This nozzle efficiency value is reasonable because it represents the total flow efficiency going from the ballast tank bladder to the exit of the spool valve, which is the greatest source of flow inefficiency. All other terms in the model were calculated using the methods presented in Sec. 5. The pitch response results are in close agreement and the depth response results show reasonable overall agreement. At 5 s, the depth response error is about 23%. It is expected that this error could be reduced with improved modeling or experimental characterization of the added mass and drag terms to better reflect the body geometry of the VBS Demo Platform.

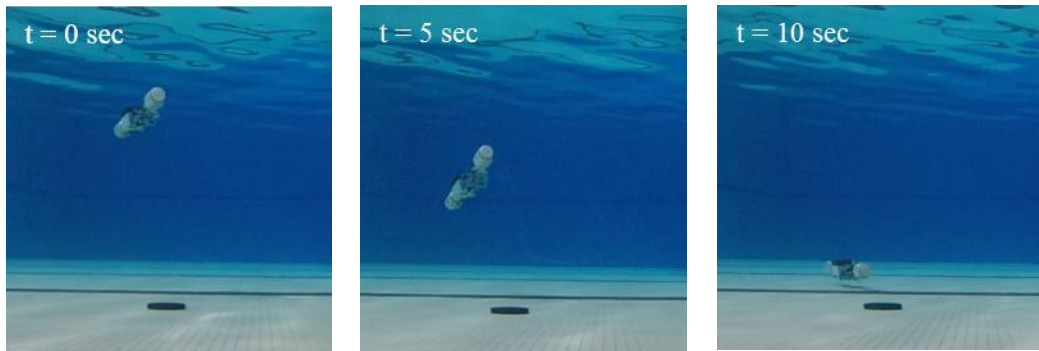


Figure 18. Descending maneuver at a nearly fixed pitch by pumping water into the fore and aft ballast tanks.

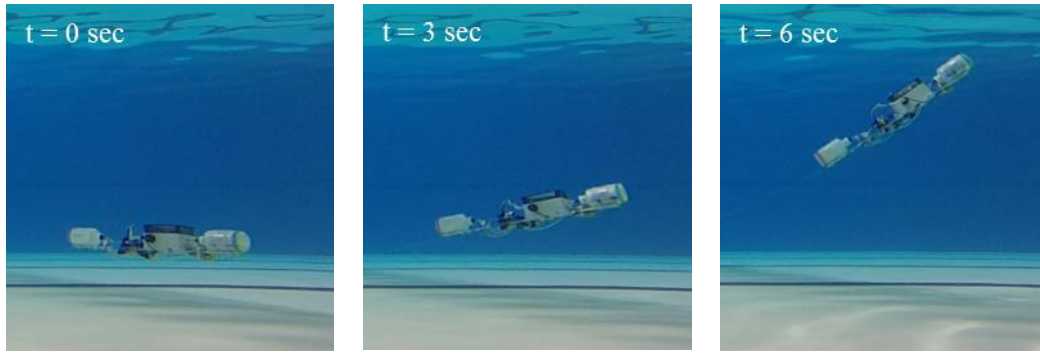


Figure 19. Pitch and depth change maneuver by venting the fore ballast tank.

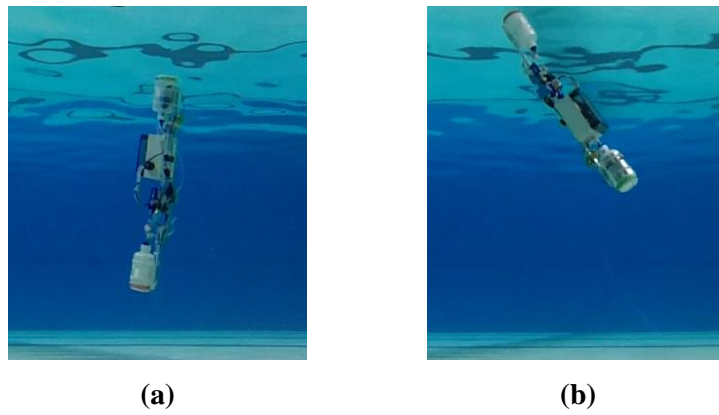


Figure 20. Extreme pitch maneuvers of (a) 83° pitch up and (b) -56° pitch down.

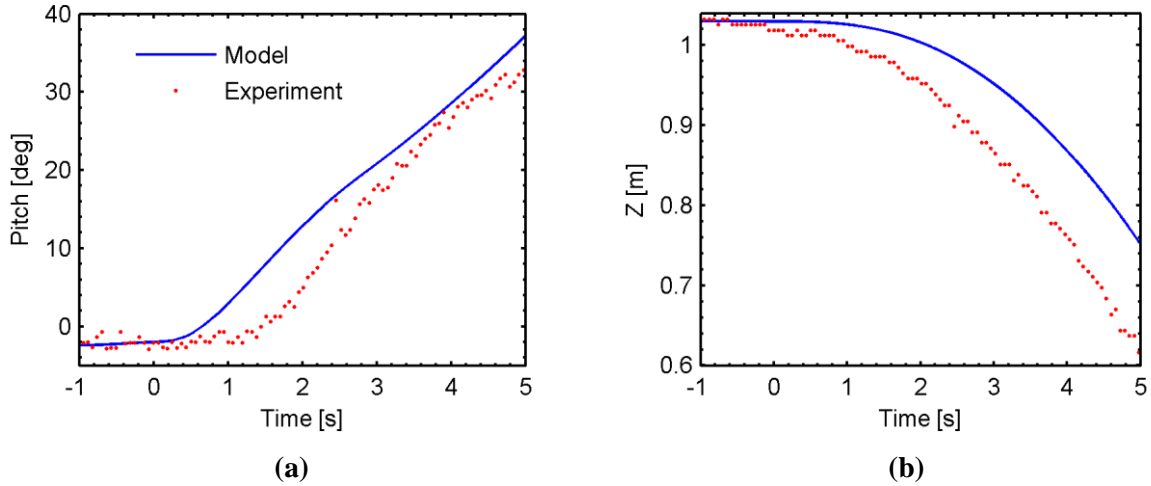


Figure 21. Experimental and predicted (a) pitch response and (b) depth response to a forward ballast tank vent command initiated at $t = 0$ sec.

9. CONCLUSIONS

This thesis has analytically investigated an active variable buoyancy system (VBS) specifically designed for multi-domain unmanned vehicles. Buoyancy systems for multi-domain unmanned vehicles have special design requirements that are unmet by conventional VBS designs. The presented VBS actuator is able to perform extreme pitch angle maneuvers that support unique multi-domain vehicle operations. The actuator design has the advantages of low weight due to the expulsion of the working fluid when inactive, high stealth due to no required air venting or recharging operations, and inherent system stability from using rigid ballast tanks and incompressible ambient water as the working fluid. The VBS is also shown to use a smaller, denser energy storage device than that of an equivalent consumable

compressed air variable buoyancy system. The design's minimal power consumption while loitering also allows for several applications, such as surveillance or evasion.

The effects of several system design parameters on the ballast tank fill rate, actuation force, energy efficiency, and vehicle dynamics were examined. Depending on the motor, applied voltage, tank precharge pressure, and tank fill fraction operation range, an optimal pump displacement exists for maximum system energy efficiency. Improving the system-level energy efficiency is critical to multi-domain vehicle design because of the need to integrate several domain-specific systems that all consume energy. Improving the energy efficiency of a single vehicle component can have a major impact on the vehicle's overall range and endurance. Vehicle simulation results show that an energy efficiency advantage during locomotion is possible through extreme pitch control, which orients the vehicle into the most streamlined position possible. The vehicle dynamics were shown to be stable in pitch and heave velocity, eliminating the need for a complicated control scheme.

A proof-of-concept platform prototype was constructed and tested to demonstrate the VBS operation concept. The prototype was able to descend while maintaining a desired, nearly fixed pitch as well as achieve a maximum pitch angle near vertical. Future work will include adding a closed-loop controller to enable automatic regulation of the vehicle pitch and depth setpoints and integrating the VBS design into a multi-domain vehicle prototype.

REFERENCES

- [1] “Russia’s Flying Submarine.” [Online]. Available: <http://www.military.com/video/aircraft/military-aircraft/russias-flying-submarine/763661806001/>.
- [2] X. Yang, T. Wang, J. Liang, G. Yao, and M. Liu, “Survey on the novel hybrid aquatic–aerial amphibious aircraft: Aquatic unmanned aerial vehicle (AquaUAV),” *Prog. Aerosp. Sci.*, vol. 74, pp. 131–151, 2014.
- [3] G. Pisanich and S. Morris, “Fielding an amphibious UAV: development, results, and lessons learned,” *Proceedings. 21st Digit. Avion. Syst. Conf.*, vol. 2, 2002.
- [4] DRS Technologies, “RQ-15 Neptune UAS,” no. 09, p. 2, 2009.
- [5] J. N. International, “All hands on deck: the sky’s the limit for shipboard UAVs.”
- [6] Kollmorgen, “Sea Sentry Organic Submarine Launched UAV.”
- [7] NRL, “Navy Launches UAV from Submerged Submarine.” [Online]. Available: <http://www.nrl.navy.mil/media/news-releases/2013/navy-launches-uav-from-submerged-submarine>.
- [8] R. Siddall and M. Kovač, “Launching the AquaMAV: bioinspired design for aerial-aquatic robotic platforms,” *Bioinspir. Biomim.*, vol. 9, p. 031001, 2014.
- [9] T. M. Wang, X. B. Yang, J. H. Liang, G. C. Yao, and W. D. Zhao, “CFD based investigation on the impact acceleration when a gannet impacts with water during plunge diving,” *Bioinspir. Biomim.*, vol. 8, p. 036006, 2013.
- [10] E. Swartz, R. Wang, C. Lamb, and A. Hoover, “Hybrid Aerial Underwater Vehicle (MIT Lincoln Lab),” 2012.
- [11] J. Liang, X. Yang, T. Wang, G. Yao, and W. Zhao, “Design and experiment of a bionic gannet for plunge-diving,” *J. Bionic Eng.*, vol. 10, no. 3, pp. 282–291, 2013.
- [12] T. Young, “Design and Testing of an Air-Deployed Unmanned Underwater Vehicle,” in *14th AIAA Aviation Technology, Integration, and Operations Conference*, American Institute of Aeronautics and Astronautics, 2014.
- [13] R. J. Lock, S. C. Burgess, and R. Vaidyanathan, “Multi-modal locomotion: from animal to application,” *Bioinspir. Biomim.*, vol. 9, p. 011001, 2014.

- [14] A. Crespi, A. Badertscher, A. Guignard, and A. J. Ijspeert, "AmphiBot I: An amphibious snake-like robot," *Rob. Auton. Syst.*, vol. 50, pp. 163–175, 2005.
- [15] A. Crespi and A. J. Ijspeert, "Online optimization of swimming and crawling in an amphibious snake robot," *IEEE Trans. Robot.*, vol. 24, no. 1, pp. 75–87, 2008.
- [16] J. Yu, R. Ding, Q. Yang, M. Tan, W. Wang, and J. Zhang, "On a bio-inspired amphibious robot capable of multimodal motion," *IEEE/ASME Trans. Mechatronics*, vol. 17, no. 5, pp. 847–856, 2012.
- [17] G. Dudek, P. Giguere, C. Prahacs, S. Saunderson, J. Sattar, L. A. Torres-Mendez, M. Jenkin, A. German, A. Hogue, A. Ripsman, J. Zacher, E. Milios, H. Liu, P. Zhang, M. Buehler, and C. Georgiades, "AQUA: An amphibious autonomous robot," *Computer (Long. Beach. Calif.)*, vol. 40, pp. 46–53, 2007.
- [18] T. Presterio, "Development of a six-degree of freedom simulation model for the REMUS autonomous underwater vehicle," *MTS/IEEE Ocean. 2001. An Ocean Odyssey. Conf. Proc. (IEEE Cat. No.01CH37295)*, vol. 1, pp. 450–455, 2001.
- [19] L. Lapierre, "Robust diving control of an AUV," *Ocean Eng.*, vol. 36, pp. 92–104, 2009.
- [20] J. Petrich and D. J. Stilwell, "Model simplification for AUV pitch-axis control design," *Ocean Eng.*, vol. 37, no. 7, pp. 638–651, 2010.
- [21] M. Caccia, R. Bono, and G. Bruzzone, "Variable-configuration UUVs for marine science applications," *IEEE Robot. Autom. Mag.*, vol. 6, no. June, pp. 22–32, 1999.
- [22] J. S. Riedel, A. J. Healey, D. B. Marco, and B. Beyazay, "Design and Development of Low Cost Variable Buoyancy System for the Soft Grounding of Autonomous Underwater Vehicles," 2005.
- [23] W. J. Kirkwood and D. E. Steele, "Active variable buoyancy control system for MBARI's ROV," *Proc. Ocean.*, vol. 2, 1994.
- [24] J. Graver, "Underwater gliders: Dynamics, control and design," p. 292, 2005.
- [25] D. C. Webb, P. J. Simonetti, and C. P. Jones, "SLOCUM: An underwater glider propelled by environmental energy," *IEEE J. Ocean. Eng.*, vol. 26, no. 4, pp. 447–452, 2001.
- [26] N. E. Leonard and J. G. Graver, "Model-based feedback control of autonomous underwater gliders," *IEEE J. Ocean. Eng.*, vol. 26, no. 4, pp. 633–645, 2001.

- [27] S. A. Woods, R. J. Bauer, and M. L. Seto, "Automated ballast tank control system for autonomous underwater vehicles," *IEEE J. Ocean. Eng.*, vol. 37, no. 4, pp. 727–739, 2012.
- [28] M. R. Clarke, "Buoyancy control as a function of the spermaceti organ in the sperm whale," pp. 27–71, 1978.
- [29] Office of Naval Research, "Submarines: How They Work - Archimedes' Principle." [Online]. Available: <http://www.onr.navy.mil/focus/blowballast/sub/work3.htm>.
- [30] S. Tangirala and J. Dzielski, "A variable buoyancy control system for a large AUV," *IEEE J. Ocean. Eng.*, vol. 32, no. 4, pp. 762–771, 2007.
- [31] Hydro Leduc, "Microhydraulics Catalogue." 2015.
- [32] Maxon Motor, "110124 Specifications," 2015. [Online]. Available: <http://www.maxonmotorusa.com/maxon/view/product/motor/dcmotor/amax/amax22/110124>.
- [33] Thunder Power RC, "Air Batteries: PROLITE + POWER SERIES 25C." [Online]. Available: <http://www.thunderpowerrc.com/>.
- [34] Guerrilla Air, "Guerrilla Air: High Performance Paintball Systems." [Online]. Available: <http://www.guerrillaair.com/>.
- [35] Luxfer, "Luxfer Gas Cylinders: SCUBA cylinders." [Online]. Available: <http://www.luxfercylinders.com/products/scuba-cylinders>.
- [36] M. Caccia, G. Indiveri, and G. Veruggio, "Modeling and identification of open-frame variable configuration unmanned underwater vehicles," *IEEE J. Ocean. Eng.*, vol. 25, no. 2, pp. 227–240, 2000.
- [37] T. I. Fossen, *Guidance and Control of Ocean Vehicles*. John Wiley & Sons, 1994.
- [38] G. Indiveri, "Modelling and Identification of Underwater Robotic Systems," 1998.
- [39] L. Jorgensen, "Prediction of Static Aerodynamic Characteristics for Space-Shuttle-Like and Other Bodies at Angles of Attack from 0 to 180," *NASA TN D-6996*, pp. 59–64, 1973.
- [40] Y. Cengel and J. Cimbala, *Fluid Mechanics: Fundamentals and Applications*, 2nd ed. McGraw-Hill, 2010.

- [41] M. Bryant, J. C. Gomez, and E. Garcia, "Reduced-Order Aerodynamic Modeling of Flapping Wing Energy Harvesting at Low Reynolds Number," *AIAA J.*, vol. 51, no. 12, pp. 2771–2782, 2013.